

**Electronic structure of $\text{Pr}_{0.67}\text{Ca}_{0.33}\text{MnO}_3$ near the Fermi level
studied by ultraviolet photoelectron and x-ray absorption
spectroscopy**

M. K. Dalai, P. Pal, and B. R. Sekhar

Institute of Physics, Sachivalaya Marg, Bhubaneswar-751005, India

N. L. Saini

Dipartimento di Fisica, Universita' di Roma "La Sapienza",

Piozzale Aldo Moro 2, 00185 Roma, Italy

R. K. Singhal and K. B. Garg

Department of Physics, University of Rajasthan, Jaipur-302004, India

B. Doyle

Laboratorio Nazionale TASC, INFN-CNR, S.S.14,

km 163.5, Area Science Park, 34012 Basovizza (TS), Italy

S. Nannarone

Laboratorio Nazionale TASC, INFN-CNR, S.S.14,

km 163.5, Area Science Park, 34012 Basovizza (TS), Italy

and Dipartimento di Ingegneria dei Materiali e dell'Ambiente,

Università di Modena e Reggio Emilia,

Via Vignolese 905, 41100 Modena, Italy

C. Martin and F. Studer

Laboratoire CRISMAT, UMR 6508, ISMRA,

Boulevard du Marechal Juin, 14050 Caen, France

Abstract

We have investigated the temperature-dependent changes in the near- E_F occupied and unoccupied states of $\text{Pr}_{0.67}\text{Ca}_{0.33}\text{MnO}_3$ which shows the presence of ferromagnetic and antiferromagnetic phases. The temperature-dependent changes in the charge and orbital degrees of freedom and associated changes in the Mn $3d$ - O $2p$ hybridization result in varied O $2p$ contributions to the valence band. A quantitative estimate of the charge transfer energy (E_{CT}) shows a larger value compared to the earlier reported estimates. The charge localization causing the large E_{CT} is discussed in terms of different models including the electronic phase separation.

PACS numbers: 79.60.-i, 75.47.Gk, 78.70.Dm, 71.20. -b

I. INTRODUCTION

Recently, a lot of attention have been focused on the charge-ordered compositions of $\text{Pr}_{1-x}\text{Ca}_x\text{MnO}_3$ due to their importance as possible prototypes for the electronic phase separation (PS) models [1, 2, 3, 4, 5, 6, 7, 8, 9] proposed to explain the phenomenon of colossal magnetoresistance (CMR). The PS models are qualitatively different from the double-exchange model [10, 11, 12] or those based on strong Jahn-Teller polarons [13, 14]. According to the PS model the ground state of CMR materials is comprised of coexisting nanosize clusters of metallic ferromagnetic and insulating antiferromagnetic nature [6]. The insulator-metal transition in this scenario is through current percolation. Though there have been a number of experimental studies showing the existence of phase separation, their size varies from nano- to mesoscopic scales [8, 9]. Radaelli et al. have shown the origin of mesoscopic phase separation to be the intergranular strain [9] rather than the electronic nature as in PS models. Nanosized stripes of a ferromagnetic phase [15] were reported in $\text{Pr}_{0.67}\text{Ca}_{0.33}\text{MnO}_3$. This compound also attracted much attention earlier due to the existence of a nearly degenerate ferromagnetic metallic state and a charge-ordered antiferromagnetic insulating state with a field-induced phase transition possible between them [16]. With slight variations in the Ca doping the $\text{Pr}_{1-x}\text{Ca}_x\text{MnO}_3$ system turns ferromagnetic ($x=0.2$) or antiferromagnetic ($x=0.4$) at low temperatures [15, 17]. The composition $x=0.33$ shows a coexistence of ferromagnetic and antiferromagnetic phases [18]. This makes the charge-orbital-ordered $\text{Pr}_{0.67}\text{Ca}_{0.33}\text{MnO}_3$ a prototype for the PS scenario.

One of the requisites for the existence of an electronic phase separation in manganites is a strong-coupling interaction affecting the hopping of the itinerant e_g electrons. The PS is expected to occur [5] when $J_H/t \gg 1$, where J_H is the Hund's coupling contribution between the localized t_{2g} and the e_g electrons and t is the hopping amplitude of the e_g electrons. The PS also favors a strong electron-phonon coupling, like the influence of a strong Jahn-Teller (JT) polaron arising from the Q_2 and Q_3 JT modes. Essentially, one expects a strong localization of charge carriers to accompany the electronic separation of phases. Apart from charge, the orbital degrees of freedom also play an important role in this scenario [5]. The itinerant electron hopping term is strongly influenced by the symmetry of the orbitals ($d_{x^2-y^2}$ and $d_{3z^2-r^2}$) hybridized with the O $2p$ orbitals of the MnO_6 octahedra. In comparison with the most popular CMR material $\text{La}_{1-x}\text{Sr}_x\text{MnO}_3$, the charge-ordered

Pr system has an inherently reduced e_g bandwidth W due to the smaller ionic radius of Pr, which also enhances the tendency for carrier localization. All these charge and orbital interactions are reflected in the near- E_F electronic structure of these materials and could be probed using electron spectroscopic techniques. Valence band photoemission and O K x-ray absorption are two such proven tools sensitive to the changes in the low-energy states crucial to these interactions. Although, there are many reports on the near- E_F electronic structure of other CMR compounds using these techniques [19, 20, 21, 22, 23, 24, 25, 26, 27, 28] only a few studies have been reported on their charge-ordered compositions [8, 29]. One of the key energy terms these spectroscopies could show earlier was the charge transfer energy E_{CT} which is intimately related to the electron-electron and electron-lattice interactions [20].

In this study we have used ultraviolet photoelectron spectroscopy and x-ray absorption spectroscopy (XAS) in order to probe the electronic structure of the occupied and unoccupied states on a well-characterized, high-quality single crystal of $\text{Pr}_{0.67}\text{Ca}_{0.33}\text{MnO}_3$. Another part of this single crystal had earlier been used for a detailed neutron scattering experiment that indicated the possible existence of a phase separation of ferromagnetic and antiferromagnetic stripes [15]. In the present study we have analyzed the temperature-dependent changes in the near- E_F electron energy states from the perspective of a phase separation.

II. EXPERIMENT

The single-crystal sample of $\text{Pr}_{0.67}\text{Ca}_{0.33}\text{MnO}_3$ was grown by the floating zone method in a mirror furnace. The compositional homogeneity of the crystal was confirmed using energy-dispersive spectroscopic analysis. Magnetization and transport measurements on this crystal showed the transition temperatures T_c and T_N to be 100 and 110 K, respectively. Details of the sample preparation, magnetization, and transport measurements and structural studies are published elsewhere [15, 30]. Angle-integrated ultraviolet photoemission measurements were performed using an Omicron μ -metal UHV system equipped with a high-intensity vacuum-ultraviolet source (HIS 13) and a hemispherical electron energy analyzer (EA 125 HR). At the He I (21.2 eV) line, the photon flux was of the order of 10^{16} photons/s/sr with a beam spot of 2.5 mm diameter. Fermi energies for all measurements were calibrated using a freshly evaporated Ag film on a sample holder. The total energy resolution, estimated from the width of the Fermi edge, was about 80 meV. The single-crystalline samples were

repeatedly scraped using a diamond file inside the chamber with a base vacuum of $\sim 1.0 \times 10^{-10}$ mbar. Scraping was repeated until negligible intensity was found for the bump around 9.5 eV, which is a signature of surface contamination [19]. For the temperature-dependent measurements, the sample was cooled by pumping liquid nitrogen through the sample manipulator fitted with a cryostat. Sample temperatures were measured using a silicon diode sensor touching the bottom of the sample holder. XAS measurements were performed using the BEAR (Ref. 31) and BACH (Ref. 32) beamlines associated with ELETTRA at Trieste, Italy. At the BEAR beamline we used monochromatized radiation from a bending magnet in order to record the O K edge spectra at room temperature and 150 K in fluorescence detection mode on a freshly scraped surface of the single crystal. The energy resolution was around 0.2 eV in the case of these two spectra. The O K edge spectra at 95 K was recorded at the BACH beamline, using the total electron yield mode. Before the measurements, the sample surface was scraped inside the UHV chamber ($\sim 1.0 \times 10^{-10}$ mbar) using a diamond file. At this beamline we used radiation from an undulator, monochromatized using a spherical grating. The resolution at the O K edge for this measurement was better than 0.1 eV.

III. RESULTS AND DISCUSSION

The angle-integrated valence band photoemission spectra of $\text{Pr}_{0.67}\text{Ca}_{0.33}\text{MnO}_3$ taken at different temperatures below and above T_c are shown in Fig. 1. Intensities of all the spectra were normalized and shifted along the y axis by a constant for clarity. The spectra, dominated by the states due to the Mn $3d$ -O $2p$ hybridized orbitals, look similar to those reported earlier on the $\text{La}_{1-x}\text{Sr}_x\text{MnO}_3$ system [19, 20, 21, 22, 23]. The origin of the two prominent features, one at ~ -3.5 eV (marked B) and another at ~ -5.6 eV (marked C) below E_F , are now well known from earlier experiments and band structure calculations [23, 24, 33] on similar systems. While the feature at -3.5 eV is mainly due to the $t_{2g\uparrow}$ states of the MnO_6 octahedra, the -5.6 eV subband has contributions from both t_{2g} and e_g states. More important contributors to the properties of these systems are the states nearer to E_F , which appear as a tail at ~ -1.2 eV (marked A) from the chemical potential. The Intensity of this feature is quite small compared to B and C and is a signature of the insulating nature of this material. Earlier photoemission experiments on $\text{La}_{1-x}\text{Sr}_x\text{MnO}_3$ also have shown that

the intensity of this tail feature A is quite small [8, 20, 21, 22, 23]. The presence of the feature A is clear from Fig. 2, where we have shown the near- E_F region of the valence band spectra taken with a higher resolution. Here, the spectra taken at different temperatures have been compared with those at room temperature. The figure also shows the difference spectra obtained by subtracting the room-temperature spectra from spectra taken at low temperatures. The feature in the difference spectra corresponds to A , which originates from the $e_{g\uparrow}$ states [22]. In order to estimate the relative changes in all the three features (A , B , and C) due to temperature, we have carefully fitted the whole valence band spectrum with three components corresponding to the three subbands contributing to this region. We used a χ^2 iterative program for fitting the different spectra with Lorentzian line shapes for A , B , and C . Except for the area of the peaks, the energy positions, widths, background, and all other parameters of all the peaks were kept the same for different temperatures. The positions and full widths at half maximum (FWHMs) of the three peaks are given in the caption of Fig. 3. The fitted spectra for 77 K (below T_c) and 300 K (above T_c) are shown on the left sides of Figs. 5(a) and 5(b) below. One can see from Figs. 3(a)-3(c) and that the area of all the peaks keeps increasing as we go down in temperature T_c , but below this temperature the intensities of both peaks C and B decrease. On the other hand, the intensity of A does not show any decrease across the transition [Fig. 3(a)].

In a reasonable approximation, the near- E_F region of the O K x-ray absorption spectra could well represent the density of unoccupied states in many of the transition metal oxide compounds [20, 34]. In order to probe the electronic structure of the unoccupied states we have performed XAS on our $\text{Pr}_{0.67}\text{Ca}_{0.33}\text{MnO}_3$ single crystal. The O K edge XAS spectra taken at room temperature and 150 and 95 K (below T_c), shown in Fig. 4, have been normalized in intensity all along the region starting from 550 eV. The preedge feature in the O K spectra (centered around 529.5 eV) is due to the strong hybridization between Mn $3d$ and O $2p$ orbitals. We will analyze this structure in detail in the later part of this paper. The broad feature around 536.5 eV is due to the bands from hybridized Pr $5d$ and Ca $3d$ orbitals, while the structure above 540 eV is due to states like Mn $4sp$ and Pr $6sp$, etc. These states are known to contribute least to the near- E_F electronic structure of these transition metal-oxide compounds. The assignments of the features mentioned above are consistent with the band structure calculations on similar systems [34, 35].

The preedge feature in the O K edge spectra carries a substantial amount of physics

involved in the properties of these materials. It has earlier been shown that the prepeak in the O K edge spectra of different CMR materials consists of two lines, one of which appears as a shoulder on the low-energy side of the other [21, 25, 27, 28]. The intensity of this shoulder was found to increase as the material goes across the insulator-metal transition [27, 28]. Since our $\text{Pr}_{0.67}\text{Ca}_{0.33}\text{MnO}_3$ sample is an insulator at all temperatures the prepeak in our O K edge spectra (Fig. 4) does not show any splitting, though the presence of the shoulder is visible as an asymmetry on the low-energy side of this peak. This shoulder feature is due to the first available unoccupied states and in XAS corresponds to the addition of an electron to the $e_{g\uparrow}$ state of the crystal-field-split MnO_6 octahedra. The main feature in the prepeak arises from the $t_{2g\downarrow}$ states [21]. For a quantitative estimate of the temperature-dependent changes in the intensities of the two features we have fitted the prepeak using two components of Lorentzian line shapes. Here also the data fitting was done using χ^2 iterative method, keeping the energy positions and widths the same for all temperatures. Results of the data fit are shown in Table I. Fitted spectra for temperatures above (300 K) and below T_c (95 K) are shown on the right side of Figs 5(a) and 5(b). Though very small, the intensity of the feature A' shows a slight increase below T_c . The best fit gives a 0.6 ± 0.1 eV difference between the energy positions of A' and B' . Following a different assignment of origin to the prepeak features Dessau *et al.* have interpreted this energy difference as a measure of the Jahn-Teller distortion ($4E_{JT}$) [26].

Having shown the temperature-dependent changes in the UPS and XAS results in Figs. 2 and 4, we present a combined picture of them in order to derive some insights into the charge transfer energy involved in the properties of the $\text{Pr}_{0.67}\text{Ca}_{0.33}\text{MnO}_3$ sample. The combined spectra of the valence band from photoemission and the preedge region of the O K edge XAS, presented in Figs 5(a) and 5(b) give the density of both occupied and unoccupied states above and below the Curie temperature (T_c). A schematic of these energy levels is shown in Fig. 6. The hole or electron doping (value of x) causes the symmetry of the last occupied and first unoccupied bands to be $e_{gz^2-r^2\uparrow}$. In Fig. 5 these states are marked by A and A' . In order to scale the left and right sides of E_F , the O K edge spectra have been shifted such that the energy of the first unoccupied state (1.4 eV from E_F) found from inverse photoemission [36] coincides with that of A' . We have used integral backgrounds for both sides of E_F and, as mentioned earlier, all the fitting parameters were kept the same including the energy positions for the high and low temperatures. The important parameter which

can be derived from this combined spectrum is the charge transfer energy E_{CT} , which is the energy required for an e_g electron to hop between the $\text{Mn}^{3+}(t_{2g}^3 e_g^1)$ and $\text{Mn}^{4+}(t_{2g}^3)$ sites. In our spectra (Fig. 5) E_{CT} is the energy difference between A and A' which corresponds to the last occupied and first unoccupied states. The value of E_{CT} is 2.6 ± 0.1 eV from our spectra, which is higher than the value (1.5 ± 0.4 eV) determined *indirectly* by Park *et al.* for the $\text{La}_{1-x}\text{Ca}_x\text{MnO}_3$ system [20]. The larger value of E_{CT} shows the existence of a stronger charge localization in the charge- or orbital-ordered $\text{Pr}_{0.67}\text{Ca}_{0.33}\text{MnO}_3$ compound.

$\text{Pr}_{0.67}\text{Ca}_{0.33}\text{MnO}_3$ shows a transition to a charge-ordered state below 220 K (T_{co}) [30, 37, 38]. Neutron diffraction studies [15] on another part of this single crystal have shown that this charge ordering turns into an antiferromagnetically structured pseudo-CE type charge or orbital ordering below 110 K. Also, the coexistence of ferromagnetic and antiferromagnetic phases below this transition temperature has been shown on this single crystal. In the pseudo-CE-type ordering the Mn $3d_{z^2-r^2}$ orbitals, where the e_g state is occupied, are aligned with the O $2p$ orbitals. Such an alignment can increase the hybridization between Mn $3d_{z^2-r^2}$ and O $2p$. Furthermore, a simultaneous decrease in the hybridization strength could also be expected for the corelike in-plane t_{2g} and O $2p$ states. The results of the curve fitting (Fig. 3) of our valence band spectra reflects these changes in hybridization with temperature. The charge ordering following the decrease in temperature causes an increase in the O $2p$ contribution to both the t_{2g} and e_g spin-up subbands in the valence region and hence the intensities of A , B , and C go up. As mentioned earlier, the pseudo-CE-type charge or orbital ordering below 110 K, results not only in a stronger hybridization of O $2p$ with the $e_{gz^2-r^2\uparrow}$ states compared to that with the t_{2g} states but a simultaneous decrease in the latter also. This is reflected in the increase in intensity of A and decrease in the intensities of both C and B below 110 K. Though in $\text{Pr}_{0.67}\text{Ca}_{0.33}\text{MnO}_3$ there is no temperature-dependent insulator-metal transition, the change in intensities of these features across T_c appears similar to the shifting of spectral weight found in the $\text{La}_{1-x}\text{Sr}_x\text{MnO}_3$ system [8].

The value of E_{CT} indicating a strong charge localization, found in our $\text{Pr}_{0.67}\text{Ca}_{0.33}\text{MnO}_3$ has significant implications for the models proposed to explain the CMR effect in manganites. Charge localization can result from strong-coupling interactions of the e_g electron with the corelike t_{2g} or the Q_2 and Q_3 Jahn-Teller modes. Both these interactions influence the electron hopping term (t). The former interaction, ferromagnetic in nature, is the Hund's coupling J_H . A large value of J_H favors the electronic separation of phases. A strong

electron-lattice coupling results from the cooperative Jahn-Teller distortions of the MnO_6 octahedra. These distortions, particularly the Q_2 and Q_3 vibrational modes of the oxygen ions are stronger in the case of Pr-containing manganites compared to La-containing ones. Park *et al.* [20] have reported a smaller charge transfer energy ($E_{CT} = 1.5$ eV) in the case of $\text{La}_{1-x}\text{Ca}_x\text{MnO}_3$ and have attributed it to small polarons (Anderson localization) induced from the ionic size difference between Mn^{3+} and Mn^{4+} . A small-polaronic model may not be able to explain the high value of E_{CT} found in $\text{Pr}_{0.67}\text{Ca}_{0.33}\text{MnO}_3$. On the other hand, a strong charge localization is expected in the case of the PS model in which the ground state is described as a mixture of ferromagnetic and antiferromagnetic regions. It is also possible that this large charge localization is due to the Zener polaron proposed by Aladine *et al.* [39]. In the Zener polaron picture, the Mn ions of adjacent MnO_6 octahedra form a dimer with variations in the Mn-O-Mn bond angle. The pseudo-CE-type charge ordering in $\text{Pr}_{1-x}\text{Ca}_x\text{MnO}_3$ favors such regular distortions in the MnO_6 octahedra. Further studies using electron spectroscopic techniques on samples in the vicinity of the charge-ordered compositions may be able to differentiate between these possible driving mechanisms behind the strong charge localization.

IV. CONCLUSIONS

Using valence band photoemission and O K edge x-ray absorption, we have probed the electronic structure of $\text{Pr}_{0.67}\text{Ca}_{0.33}\text{MnO}_3$, which is regarded as a prototype for the electronic phase separation models in CMR systems. With decrease in temperature the O $2p$ contributions to the t_{2g} and e_g spin-up states in the valence band were found to increase until T_c . Below T_c , the density of states with e_g spin-up symmetry increased while those with t_{2g} symmetry decreased, possibly due to the change in the orbital degrees of freedom associated with the Mn $3d$ - O $2p$ hybridization in the pseudo-CE-type charge or orbital ordering. These changes in the density of states could well be connected to the electronic phase separation reported earlier. Our quantitative estimate of the charge transfer energy (E_{CT}) is 2.6 ± 0.1 eV, which is large compared to the earlier reported values in other CMR systems. Such a large charge transfer energy may support the phase separation model.

ACKNOWLEDGMENTS

The authors would like to thank the staff at the BEAR and BACH beamlines of Elettra Sincrotrone Trieste, Italy for the XAS measurements and DST, India for financial support.

- [1] I. G. Deac, J. F. Mitchell and P. Schiffer Phys. Rev. B **63**, 172408 (2001).
- [2] L. M. Fisher, A. V. Kalinov, I. F. Voloshin, N. A. Babushkina, K. I. Kugel, and D. I. Khomskii Phys. Rev. B **68**, 174403 (2003).
- [3] R. Kajimoto, H. Mochizuki, H. Yoshizawa, S. Okamoto, and S. Ishihara, Phys. Rev. B **69**, 54433 (2004).
- [4] K. S. Nagapriya, A. K. Raychoudhuri, B. Bansal, V. Venkataraman, S. Parashar, and C. N. R. Rao, Phys. Rev. B **71**, 024426 (2005).
- [5] A. Moreo, S. Yunoki, and E. Dagatto, Science **283**, 2034 (1999).
- [6] A. Moreo, M. Mayr, A. Feiguin, S. Yunoki, and E. Dagotto, Phys. Rev. Lett. **84**, 5568 (2000).
- [7] S. Yunoki, J. Hu, A. L. Malvezzi, A. Moreo, N. Furukawa, and E. Dagotto, Phys. Rev. Lett. **80**, 845 (1998).
- [8] D. D. Sarma, D. Topwal, U. Manju, S. R. Krishnakumar, M. Bertolo, S. La Rosa, G. Cautero, T. Y. Koo, P. A. Sharma, S.-W. Cheong, and A. Fujimori, Phys. Rev. Lett. **93**, 97202 (2004).
- [9] P. G. Radaelli, R. M. Ibberson, D. N. Argyriou, H. Casalta, K. H. Andersen, S. -W. Cheong and J. F. Mitchell, Phys. Rev. B **63**, 172419 (2001)
- [10] C. Zener, Phys. Rev. **82**, 403 (1951).
- [11] P. W. Anderson and H. Hasegawa, Phys. Rev. **100**, 675 (1955).
- [12] P. -G. de Gennes, Phys. Rev. **118**, 141 (1960).
- [13] A. J. Millis, P. B. Littlewood, and B. I. Shraiman, Phys. Rev. Lett. **74**, 5144 (1995).
- [14] A. J. Millis, B. I. Shraiman, and R. Mueller Phys. Rev. Lett. **77**, 175 (1996).
- [15] Ch. Simon, S. Mercone, N. Guiblin, C. Martin, A. Brulet, and G. Andre, Phys. Rev. Lett. **89**, 207202 (2002).
- [16] K. Miyano, T. Tanaka, Y. Tomioka, and Y. Tokura, Phys. Rev. Lett. **78**, 4257 (1997).
- [17] E. O. Wollan, and W. C. Koehler, Phys. Rev. **100**, 545 (1955)
- [18] Z. Jirak, S. Krupicka, Z. Simsa, M. Dlouha, and S. Vratilav, J. Magn. Magn. Mater. **53**, 153

(1985)

- [19] D. D. Sarma, N. Shanthi, S. R. Krishnakumar, T. Saitoh, T. Mizokawa, A. Sekiyama, K. Kobayashi, A. Fujimori, E. Weschke, R. Meier, G. Kaindl, Y. Takeda, and M. Takano, *Phys. Rev. B* **53**, 6873 (1996).
- [20] J.-H. Park, C. T. Chen, S. W. Cheong, W. Bao, G. Meigs, V. Chakarian, and Y. U. Idzerda, *Phys. Rev. Lett.* **76**, 4215 (1996)
- [21] J.-H. Park, T. Kimura, and Y. Tokura, *Phys. Rev. B* **58**, R13330 (1998).
- [22] T. Saitoh, A. E. Bocquet, T. Mizokawa, H. Namatame, A. Fujimori, M. Abbate, Y. Takeda, and M. Takano, *Phys. Rev. B* **51**, 13942 (1995).
- [23] T. Saitoh, A. Sekiyama, K. Kobayashi, T. Mizokawa, A. Fujimori, D. D. Sarma, Y. Takeda, and M. Takano, *Phys. Rev. B* **56**, 8836 (1997).
- [24] P. Pal, M. K. Dalai, B. R. Sekhar, S. N. Jha, S. V. N. Bhaskara Rao, N. C. Das, C. Martin, and F. Studer, *J. Phys.: Condens. Matter* **17**, 2993 (2005).
- [25] D. S. Dessau, Y. D. Chuang, A. Gromko, T. Saitoh, T. Kimura, and Y. Tokura, *J. Electron Spectrosc. and Relat. Phenom.* **117-117**, 265 (2001).
- [26] D. S. Dessau, T. Saitoh, C.-H. Park, Z.-X. Shen, Y. Moritomo, and Y. Tokura, in *Science and Technology of Magnetic Oxides*, edited by M. Hundley, J. Nickel, R. Ramesh, and Y. Tokura, MRS Symposia Proceedings No. 494 (Materials Research Society, Pittsburgh, 1998), p. 181.
- [27] N. Mannella, A. Rosenhahn, M. Watanabe, B. Sell, A. Nambu, S. Ritchey, E. Arenholz, A. Young, Y. Tomioka, and C. S. Fadley, *Phys. Rev. B* **71**, 125117 (2005).
- [28] O. Toulemonde, F. Millange, F. Studer, B. Raveau, J. H. Park, and C. T. Chen, *J. Phys. Condens. Matter* **11**, 109 (1999).
- [29] J.-H. Park, C. T. Chen, S.-W. Cheong, W. Bao, and G. Meigs, *J. Appl. Phys.* **79**, 4558 (1996).
- [30] S. Mercone, V. Hardy, C. Martin, Ch. Simon, D. Saurel, and A. Brulet, *Phys. Rev. B* **68**, 094422 (2003).
- [31] S. Nannarone, F. Borgatti, A. DeLuisa, B. P. Doyle, G. C. Gazzadi, A. Giglia, P. Finetti, N. Mahne, L. Pasquali, M. Pedio, G. Selvaggi, G. Naletto, M. G. Pelizzo, and G. Tondello, in *SYNCHROTRON RADIATION INSTRUMENTATION: Eighth international conference on synchrotron radiation instrumentation*, edited by T. Warwick, J. Stohr, H. A. Padmore, and J. Arthur, AIP Conf. Proc. No. 705 (AIP, San Francisco, California, 2003), pp. 450-453.

- [32] M. Zangrando, M. Finazzi, G. Paolucci, G. Comelli, B. Diviacco, R. P. Walker, D. Cocco, and F. Parmigiani, *Rev. Sci. Instrum.* **72**, 1313 (2001).
- [33] E. Z. Kurmaev, M. A. Korotin, V. R. Galakhov, L. D. Finkelstein, E. I. Zabolotzky, N. N. Efremova, N. I. Lobachevskaya, S. Stadler, D. L. Ederer, T. A. Callcott, L. Zhou, A. Moewes, S. Bartkowski, M. Neumann, J. Matsuno, T. Mizokawa, A. Fujimori, and J. Mitchell, *Phys. Rev. B* **59**, 12799 (1999).
- [34] F. M. F. de Groot, M. Grioni, J. C. Fuggle, J. Ghijsen, G. A. Sawatzky, and H. Petersen, *Phys. Rev. B* **40**, 5715 (1989).
- [35] H. Kurata, E. Lefevre, C. Colliex, and R. Brydson, *Phys. Rev. B* **47**, 13763 (1993).
- [36] A. Chainani, M. Mathew, and D. D. Sarma, *Phys. Rev. B* **47**, 15397 (1993).
- [37] C. Martin, A. Maignan, M. Hervieu, and B. Raveau, *Phys. Rev. B* **60**, 12191 (1999).
- [38] V. Hardy, A. Wahl, and C. Martin, *Phys. Rev. B* **64**, 64402 (2001)
- [39] A. Daoud-Aladine, J. Rodriguez-Carvajal, L. Pinsard-Gaudart, M. T. Fernandez-Diaz, and A. Revcolevschi, *Phys. Rev. Lett.* **89**, 097205 (2002).

TABLE I: χ^2 iterative fitting parameters for the preedge peak in O *K* XAS. The intensities of *B'* and *A'* at low temperature are normalized with respect to the total intensity of the prepeak at room temperature. We have used an integral background, which was kept the same for all the spectra. The energy positions and FWHMs were determined by finding the best fit common to the three spectra by a χ^2 iterative program. The final fit for all the spectra from different temperatures were obtained with the same energy positions and FWHMs.

Temperature (K)	O <i>K</i> edge x-ray absorption spectra					
	<i>B'</i>			<i>A'</i>		
	Position (eV)	FWHM (eV)	Normalized area	Position (eV)	FWHM (eV)	Normalized area
95	2.11	1.52	0.72	1.48	0.97	0.29
150	2.11	1.52	0.72	1.48	0.97	0.26
300	2.12	1.52	0.73	1.47	0.97	0.26

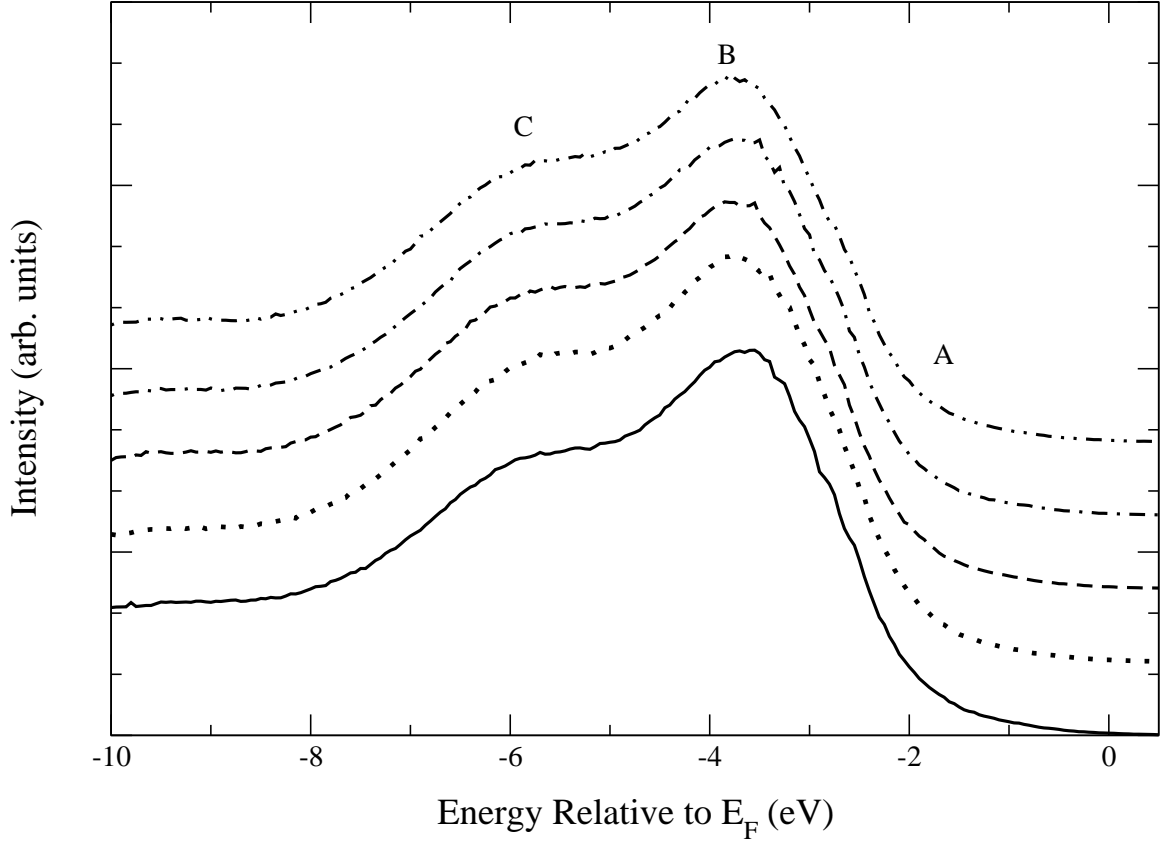


FIG. 1: Valence band photoemission spectra of $\text{Pr}_{0.67}\text{Ca}_{0.33}\text{MnO}_3$ taken using He *I* photon energy (21.2 eV) at 77 (solid line), 110 (dotted), 150 (dashed), 220 (dot-dashed), and 300 K (double-dot dashed). All the spectra have been normalized and shifted along y-axis by a constant for clarity. The subbands around -1.2 ($e_{g\uparrow}$), -3.5 ($t_{2g\uparrow}$), and -5.6 eV ($e_{g\uparrow} + t_{2g\uparrow}$) are marked as *A*, *B*, and *C* respectively.

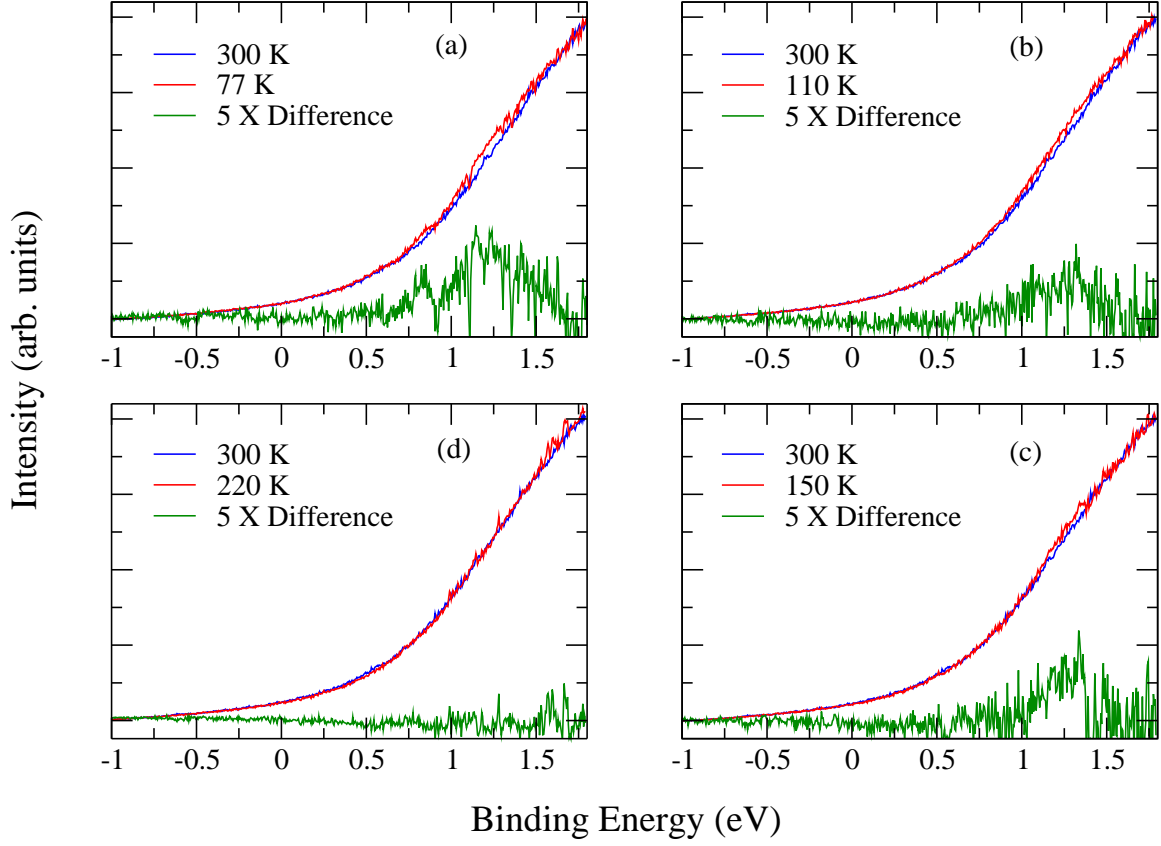


FIG. 2: (color online) High-resolution photoemission spectra of the near- E_F region of the valence band of $\text{Pr}_{0.67}\text{Ca}_{0.33}\text{MnO}_3$. In (a) the spectrum taken below T_c (red) is compared with the normal state (300 K) spectrum (blue). The difference spectrum (green) obtained by subtracting the spectra at 300 K from 77 K and multiplied by 5 is also shown in the panel. Similarly, in (b), (c), and (d) the near- E_F spectra taken at 110, 150, and 220 K are compared with that taken at 300 K. The feature in the difference spectra corresponds to the tail feature $A(e_{g\uparrow})$ in Fig. 1.

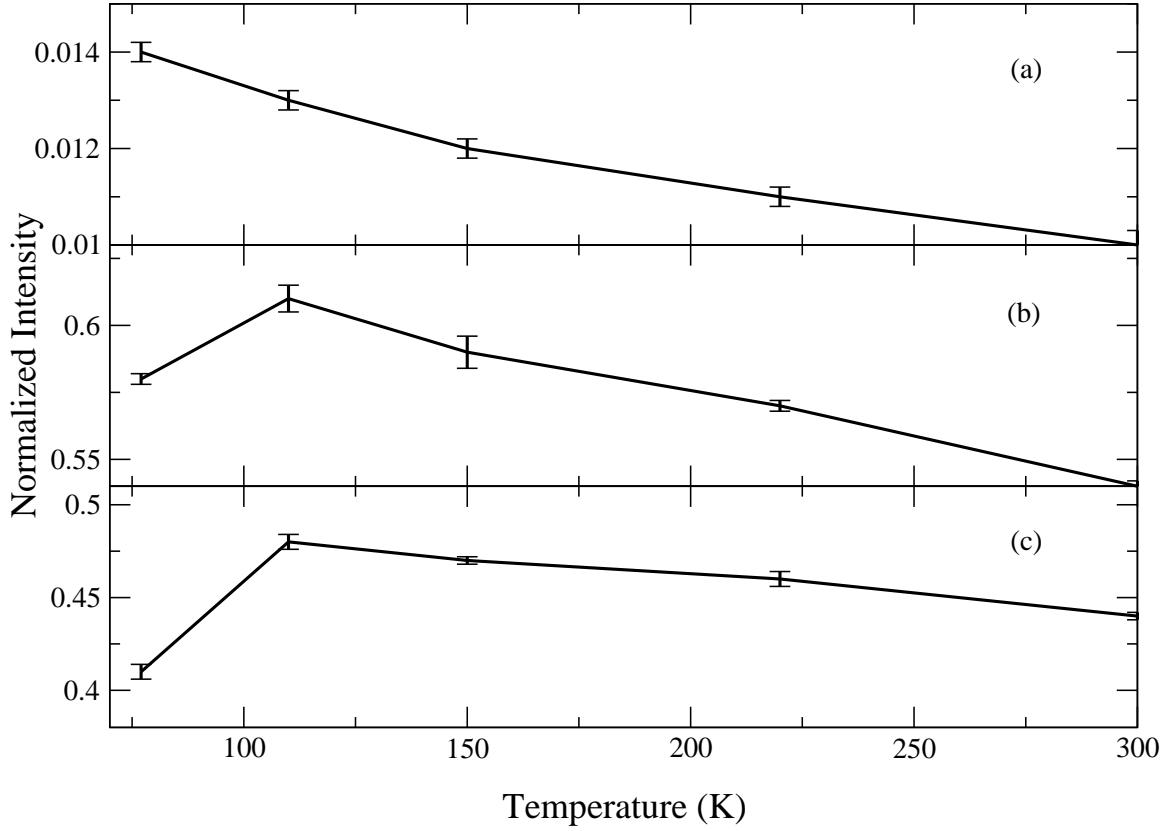


FIG. 3: Temperature dependence of the area of the three valence band features obtained from fitting the spectra with Lorentzian line shapes using a χ^2 iterative program. We have used an integral background, which was kept the same for all the spectra. The energy positions and FWHMs were determined by finding the best fit common to all the spectra by the iterative program. The final fit for all spectra at different temperatures were obtained with the same energy positions and FWHMs. (a), (b), and (c) correspond to the features *A*, *B*, and *C* positioned at -1.19, -3.49, and -5.63 eV with FWHMs 2.56, 1.93, and 1.37 eV, respectively.

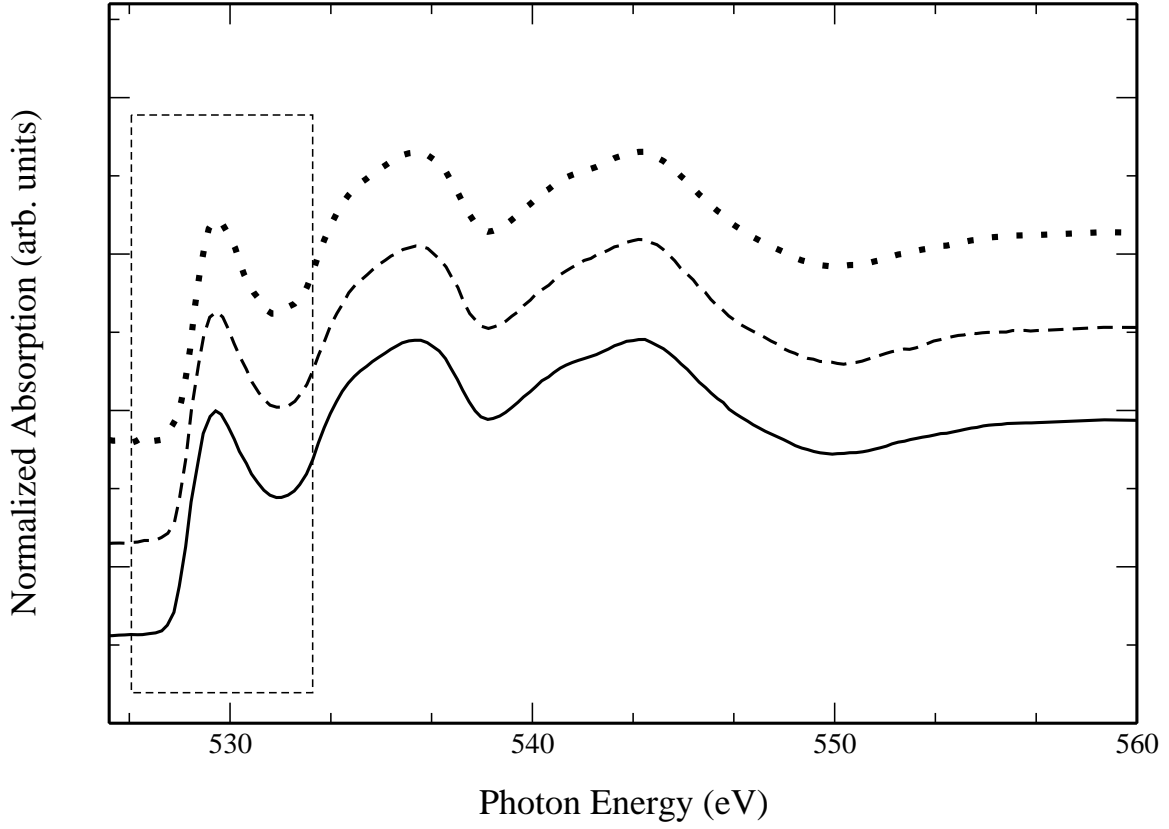


FIG. 4: O K edge x-ray absorption spectra of $\text{Pr}_{0.67}\text{Ca}_{0.33}\text{MnO}_3$ taken at 300 (solid line), 150 (dashed line), and 95 K (dotted). The preedge feature centered around 529.5 eV (marked by a box) is where most interest lies. Since this feature consists of two peaks (a main line and a shoulder on the low-energy side), this part of the spectrum was fitted with two components of Lorentzian line shapes. Results of the curve fit are given in Table I.

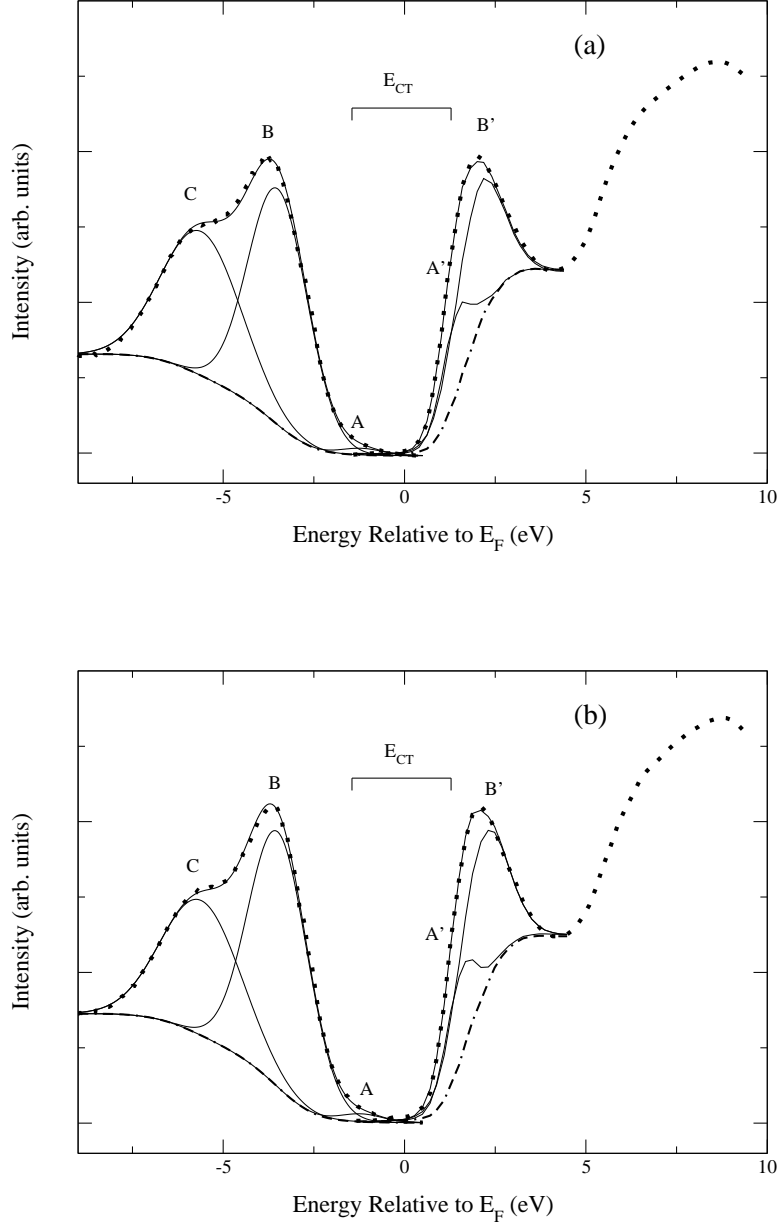


FIG. 5: (a) Combined spectra from valence band photoemission (occupied energy states) and prepeak in O K edge x-ray absorption spectra (unoccupied energy states) of $\text{Pr}_{0.67}\text{Ca}_{0.33}\text{MnO}_3$ taken at room temperature (above T_c). The three features corresponding to the subbands in the valence region are marked A , B , and C . The two peaks of the fitted O K edge prepeak are marked A' and B' . We used integral background for both sides of E_F . Details of the fitting are mentioned in the text. (b) Combined spectra of $\text{Pr}_{0.67}\text{Ca}_{0.33}\text{MnO}_3$ below T_c . The valence band spectrum was taken at 77 K and O K edge XAS was taken at 95 K.

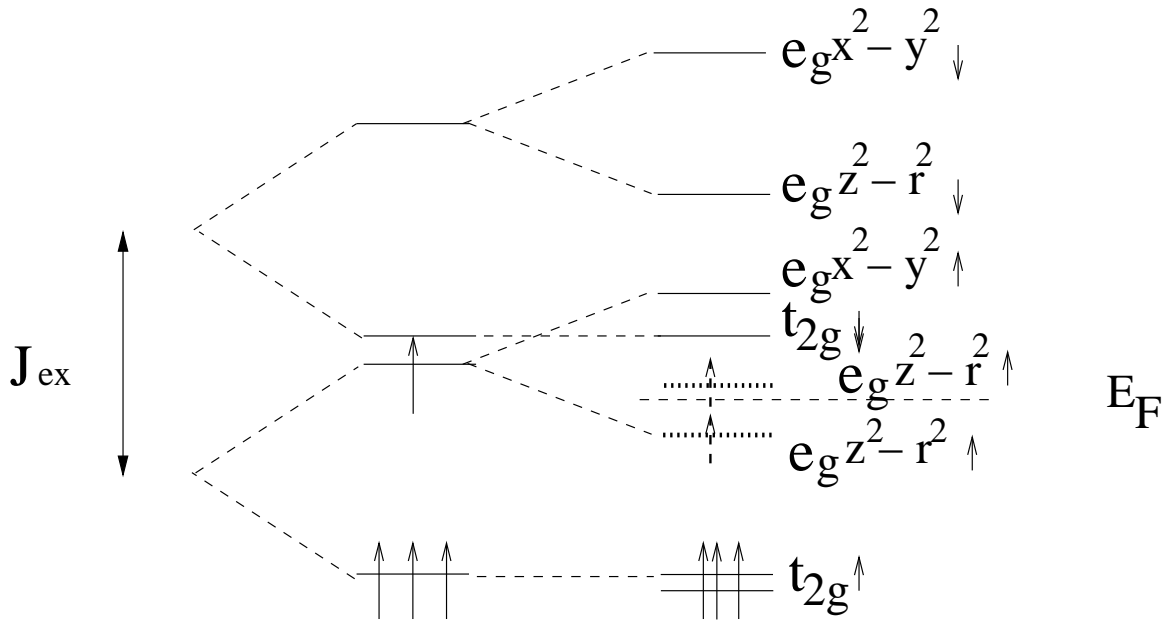


FIG. 6: Schematic diagram of the near- E_F energy levels of $\text{Pr}_{0.67}\text{Ca}_{0.33}\text{MnO}_3$ in the occupied and unoccupied parts. The diagram is not drawn to scale. Some of the $e_{g\uparrow}$ states are occupied (at the Mn^{3+} sites) and some are unoccupied (at the Mn^{4+} sites). Hence the last occupied and first unoccupied states are marked with dotted lines.